Fuel 306 (2021) 121736

Contents lists available at ScienceDirect

Fuel

journal homepage: www.elsevier.com/locate/fuel

Full Length Article

What physicochemical properties of biochar facilitate interspecies electron transfer in anaerobic digestion: A case study of digestion of whiskey by-products

Chen Deng [a,b], Richen Lin [a,b,*], Xihui Kang [a,b], Benteng Wu [a,b], David M Wall [a,b], Jerry D Murphy [a,b]

[a] MaREI Centre, Environmental Research Institute, University College Cork, Cork, Ireland
[b] Civil, Structural and Environmental Engineering, School of Engineering and Architecture, University College Cork, Cork, Ireland

ARTICLE INFO

Keywords:
Biomethane
Anaerobic digestion
Biochar
Direct interspecies electron transfer

ABSTRACT

The efficiency of microbial interspecies electron transfer between syntrophic bacteria and methanogens is considered a rate-limiting factor for the overall efficiency of anaerobic digestion (AD). Stimulating interspecies electron transfer by biochars has been demonstrated to be efficient to enhance AD. However, the enhancing effects vary significantly depending on biochar properties. The correlations between them are not fully understood. Herein, biochars with different physicochemical properties were produced from a whiskey by-product "draff" and subsequently applied in the digestion of draff. The biochar produced at 700 °C statistically (p less than 0.05) enhanced biomethane yield by 5%. In contrast, biochars produced at 500 and 900 °C did not increase biomethane yield. The addition of 700 °C-derived biochar in AD increased the relative abundance of the methanogen *Methanosarcina*, which may be the electron-accepting partner in direct interspecies electron transfer (DIET). The enrichment of *Methanosarcina* suggested the potential shift of the interspecies electron transfer pathway towards the DIET mode. The characterization of biochar properties suggested that moderate graphitization degree and abundant active surface functional groups (such as –C═O, pyridinic-N, and graphitic-N) were correlated with a more stimulating interspecies electron transfer through both the carbon matrices and the charging – discharging cycles of surface functional groups.

1. Introduction

Anaerobic digestion (AD) is an established technology for biogas recovery whilst treating a wide array of organic substrates (such as agri-food by-products). These substrates are degraded by consortia of bacteria and archaea to produce biogas, which can subsequently be upgraded to biomethane. The significance of biomethane as an advanced biofuel for transport has been well demonstrated and recognized worldwide [1,2]. China, which currently produces almost a third of global biogas, aims to expand biogas production 2.5-fold by 2030 [3] with ambitions to provide renewable energy and reduce air pollution whilst improving waste management practices. The European Union proposes a binding target of 14% renewable energy share and a sub-target of 3.5% advanced biofuels share in transport consumption by 2030 [4]. However, by December 2020 advanced biofuels have a market share of less than 0.5% of energy in transport [5]. Biomethane has great potential in the hard to abate sector of heavy transport [6]. Therefore, the production of advanced biofuels such as biomethane is incentivized to be enhanced and refined to optimize the system; this optimization includes the energy yield from specific feedstocks and an increase in the range of sustainable feedstocks for advanced biofuel production.

Whiskey manufacturing processes generate large quantities of by-products which necessitate energy-intensive post-treatment (including segregation and evaporation) to form traditional valuable products such as animal feed. Meanwhile, these whiskey by-products have a significant potential for biomethane production due to their high content of carbohydrates and proteins. A previous study of a large distillery has suggested that biogas from distillery by-products can replace up to 64% of natural gas consumption onsite and lead to a 54% reduction in direct greenhouse gas emissions [7]. As a typical solid by-product, draff primarily consists of cellulose, hemicellulose, lignin and proteins. The high cellulose and hemicellulose content of draff suggests it as a promising feedstock for

* Corresponding author at: MaREI Centre, Environmental Research Institute, University College Cork, Ireland.
E-mail address: richen.lin@ucc.ie (R. Lin).

https://doi.org/10.1016/j.fuel.2021.121736
Received 2 July 2021; Received in revised form 11 August 2021; Accepted 13 August 2021
Available online 26 August 2021

biomethane production. However, the considerable lignin content in draff may hinder the degradation of cellulose and hemicellulose, which on the contrary makes it a good feedstock for biochar production through pyrolysis. Lignin-rich digested stillage is also a good candidate to produce high-quality biochar which could constitute attractive soil amendments in a carbon-negative biorefinery [8]. Thus, it may be that draff is feasible to produce advanced biomethane and/or as carbonaceous biochar that when applied to land can generate negative emissions through enhanced photosynthesis in a circular bioenergy system [9,10].

Despite the potential for biomethane production, digestion of draff is still challenged by the low conversion efficiency and the instability in AD due to its recalcitrant structure. Interspecies electron transfer between the syntrophic bacteria and methanogenic archaea is a fundamental factor in determining the overall AD efficiency. Interspecies electron transfer can be achieved through either a mediated interspecies electron transfer (MIET) or a direct interspecies electron transfer (DIET) pathway. DIET has been demonstrated to be more efficient than MIET as it is not limited by the diffusion rate of electron carriers such as hydrogen and formate [11]. DIET-based syntrophy can naturally take place via cytochromes/pili and can also be engineered via the addition of conductive materials such as graphene, activated carbon, magnetite, and biochar [12–14]. In recent studies, biochar has shown encouraging effects on enhancing AD performance through stimulating DIET [15–18]. These findings highlight future applications of biochar in AD and the bridging role of biochar between biological and thermochemical conversion processes in a cascading circular bioenergy system [19].

However, the literature is not definitive on the benefits of biochar addition to AD systems. Table 1 summarizes the recent studies focusing on the effects of biochars with different properties in mesophilic AD. The impacts on biomethane yield were categorized into three types: positive (increase in biomethane yield $\geq$ 10%), neutral (0 $\leq$ increase in biomethane yield $\leq$ 9%), and negative (increase in biomethane yield less than 0). The variable impacts of biochars are highly dependent on their properties [20]. Biochar made from the same biomass resource can lead to either positive or neutral impacts on biomethane yield due to the differences arising from different pyrolysis temperatures [21]. The potential to facilitate interspecies electron transfer is an important factor that determines the effects of biochar. It was speculated that the electron-donating and accepting capacity of biochar, which is associated with the surface chemical properties of biochar, might determine the capacity of biochar in promoting interspecies electron transfer [22,23]. Besides the stimulation of interspecies electron transfer, the surface properties of biochar also impact biochar's other effects on AD such as inhibitor adsorption, pH buffering, and immobilization of microorganisms [24]. These important surface properties include the surface microstructure, pore volume and size, specific surface area, and surface functional groups. However, arguments still exist over the optimal biochar properties for enhancing AD performance. Wang et al. considered the redox activity of biochar as the decisive property for promoting biomethane production [21]. Ren et al. suggested that it was the abundance of surface oxygen-containing functional groups rather than the total redox properties that impacted the biomethane production [25]. Overall, the gap in the state of the art may be said to be the understanding of how the properties of biochar correlate to its facilitation of and promotional effects on AD. Therefore, the determination of the exact properties of biochar is crucial for a full understanding of the mechanism of interspecies electron transfer and of how to engineer biochar-enhancing AD.

The innovation of this study is the identification of the key properties which contribute to the facilitating effects of biochar on biomethane production. The specific objectives are to (1) produce high-quality biochar from the whiskey by-product draff; (2) evaluate the effects of draff-derived biochar on biomethane production; and (3) identify the crucial properties of biochars that have great effects on biomethane production in AD. To achieve these objectives, the draff was pyrolyzed at different temperatures to produce biochars with various properties. The properties of biochars were identified in terms of the specific surface area, porosity, crystallinity of carbon structure, and surface functional groups. A biomethane potential assay was carried out to evaluate the effects of different biochars on biomethane production.

2. Materials and methods

2.1. Materials

The draff feedstock was sourced from a local whiskey distillery in Ireland. The compositional characteristics of draff are listed in Table 2. The original draff was used as received for the biomethane potential assay, but it was oven-dried at 105 °C overnight before being used as the feedstock for biochar production.

Three types of biochar were produced through pyrolysis of draff at 500, 700, and 900 °C in a compact tube furnace (R50/250/12, Nabertherm, Germany). Under N_2 atmosphere, draff was firstly heated up to the set temperature at a ramp rate of 10 °C/min, then kept at the set temperature for an hour, and finally cooled down to the room temperature. Corresponding to the pyrolysis temperature, the obtained biochars were referred to as Char_500, Char_700, and Char_900, respectively. The obtained biochars were ground into powders and sieved to diameters below 150 μm. Biochar samples were sealed in plastic bags and kept in a desiccator before use.

The inoculum for the biomethane potential assay was sourced from a local biogas plant treating food waste and it was acclimatized in the laboratory using cellulose and peptone as feedstock for several weeks. The inoculum was degassed for a week before use in the biomethane potential assay. The compositional characteristics of the inoculum are listed in Table 2.

2.2. Biomethane potential assay

A batch biomethane potential assay was conducted in a Bioprocess Automatic Methane Potential Test System (APMTS II, Bioprocess Control, Sweden). A detailed introduction of the AMPTS II and its operation procedure can be found in a previous paper [18]. Five groups of digestion (G0–G4) were conducted in triplicate. In the control group G0, 9.77 g of wet draff feedstock (containing 3.00 g VS) and 247.32 g of inoculum (containing 6.00 g VS) were added to each reactor. G1, G2 and G3 were three biochar amended digestion groups with the addition of Char_500, Char_700, and Char_900, respectively.

A previous literature review on biochar addition in batch AD experiments provided references for the determination of biochar dosage in this study [18]. In the biochar amended groups, 0.75 g of biochar powder (equivalent to 25% of the volatile solids in the feedstock) was added into each reactor in addition to 9.77 g of draff and 247.32 g of inoculum. G4 was a blank group containing only 247.32 g of inoculum to evaluate the contributory effect of the inoculum. Biomethane yield in G0 to G3 was corrected by the yield in the blank group G4 to offset the contributory of the inoculum. After the loading of feedstock, inoculum, and biochar, the working volume of each reactor was adjusted to 400 ml with distilled water. The initial pH in the reactor was measured as 8.06 $\pm$ 0.00, 8.05 $\pm$ 0.01, 8.03 $\pm$ 0.01, 8.04 $\pm$ 0.01, and 8.13 $\pm$ 0.00 for G0 to G4, respectively. The digestion was carried out at 37 °C for 30 days. The effluent in each reactor was sampled every three days for the analysis of volatile fatty acids (VFAs). The VFAs concentration in the effluents was quantified using a gas chromatography system (Agilent 7890B, USA). Equipment configuration of the gas chromatography system and analyzing method were described in a previous paper [33]. The VFAs concentration on the starting day (day 0) was set as the baseline and subtracted from the yield of VFAs.

The statistical analysis of differences in biomethane production was conducted on the software IBM SPSS Statistics V25 using the one-way ANOVA method. It was considered that there were significant differences when $p < 0.05$.

Table 1
A summary of studies focusing on effects of different biochars on biomethane yield in mesophilic anaerobic digestion (AD) process.

AD Feedstock	Biochar source	Pyrolysis temperature(°C)	Molar O/C	Molar H/C	C Content (%)	H content (%)	O content (%)	N content (%)	SSA (m^2/g)	EC(μS/cm)	EDC (mmol/g)	Increase in CH_4 yield	Impact	Reference
Sludge	Corn stover	300	0.21	0.76	61.1	3.9	17.5	1.4	19.8	800,000	0.598	31%	Positive (+)	[21]
		500	0.13	0.46	64.8	2.5	10.9	1.2	20.1	0.7	0.313	11%	Positive (+)	
		700	0.06	0.28	72.9	1.7	2.4	0.7	32.8	1,010,000	0.228	4%	Neutral (\)	
Wastewater sludge	Douglas fir	400	0.36	0.48	65.1	2.6	31.3	0.0	17.0	468		11%	Positive (+)	[26]
		500	0.24	0.33	72.7	2.0	23.8	0.1	13.2	499		11%	Positive (+)	
		600	0.15	0.27	78.9	1.8	15.9	0.5	18.4	512		10%	Positive (+)	
		730	0.15	0.04	80.3	0.2	16.1	0.1	18.4	636		10%	Positive (+)	
Food waste	Soft wood	700							162.3	160		9%	Positive (+)	[27]
	Soft wood	550							26.4	90		5%	Neutral (\)	
	Oil seed rape	700						1.3	25.2	3110		15%	Positive (+)	
	Wheat straw	550						1.4	26.4	1700		24%	Positive (+)	
Aqueous phase of bio-oil from algae	Canola meal	700								180 (S)		80%	Positive (+)	[28]
	Canola meal	900								273 (S)		54%	Positive (+)	
	Switchgrass	500							5.7	338 (S)		72%	Positive (+)	
	Ashe Juniper	400							8.0	350 (S)		1133%	Positive (+)	
	Ashe Juniper	600								60 (S)		266%	Positive (+)	
Raw straw and cow manure	Rice husk	600	0.78	0.21	48.2	0.8	50.4	0.5	2.0			5%	Neutral (\)	[29]
	Shrub	600	0	3.98	65.7	21.8	0	10.8	14.7			7%	Neutral (\)	
	Peanut shell	600	0.33	0.52	65.6	2.8	28.9	2.2	0.6			5%	Neutral (\)	
	Straw	600	0.52	0.26	57.4	1.2	39.8	1.4	1.0			10%	Positive (+)	
	Sawdust	600	0.91	9.08	27.0	20.4	32.7	1.9	1.3			3%	Neutral (\)	
	Coconut shell	600	0.83	3.93	39.1	12.8	43.0	4.5	774.5			13%	Positive (+)	
	Tar	600	0.35	0.83	64.0	4.4	29.9	1.5	34.7			7%	Neutral (\)	
Sorghum	Rice husk	600	0.10	0.28	33.9	0.8	4.5	0.2				0	Neutral (\)	[30]
Glucose	Rice straw	500	0.48	0.52	58.6	2.6	37.7	1.2	77.1	7.37	0	1%	Neutral (\)	[22]
	Corn stalk	500	0.43	0.51	61.3	2.6	35.5	0.6	18.4	16.29	0.001	−3%	Negative (−)	
	Bamboo	500	0.11	0.44	84.0	3.1	12.5	0.4	207.8	57.88	0.018	2%	Neutral (\)	
Food waste	Fine walnut shell	900	0.06	0.20	47.0	0.8	3.9	0.8	86.5			−73% – 0	Negative (−)	[31]
Municipal solid waste	Rice straw	500			59.4				5.5			−47%	Negative (−)	[32]

Note: SSA = specific surface area, EC = electrical conductivity, EDC = electron-donating capacity. (S) means the EC was measured in biochar suspensions.

Table 2
Characteristics of draff and inoculum.

	Draff	Inoculum
Proximate analysis		
TS (wwt%)	31.7 ± 0.1	3.9 ± 0.0
VS (wwt%)	30.7 ± 0.1	2.4 ± 0.0
Ash (wwt%)	1.0 ± 0.0	1.4 ± 0.0
Moisture (wwt%)	68.3 ± 0.1	96.1 ± 0.0
VS/TS	96.8	61.5
Ultimate analysis		
C (% VS)	51.8 ± 0.0	\
H (% VS)	6.8 ± 0.0	\
N (% VS)	4.2 ± 0.2	\
O (% VS)	37.2 ± 0.3	\
C/N	12.3	\
Energy content		
HHV (kJ/g VS)	20.6	\
Theoretical biomethane potential (ml/g VS)	517.7[a]	\

Note: TS = total solid, VS = volatile solid, HHV = higher heating value. [a] Calculated based on the Buswell equation Eq. (3).

2.3. Biomass and biochar characterization

The weight percentages of total solids (TS), volatile solids (VS), ash, and moisture in draff and inoculum were measured according to the 2540G standard methods [34]. The weight percentage of each element (carbon, hydrogen, and nitrogen) in the TS was measured by an elemental analyzer (Exeter Analytical, CE 440 Model); these were subsequently converted to a VS basis using the VS/TS ratio. The higher heating value (HHV) of the draff and biochars was calculated from the elemental composition data using the modified Dulong Formula as described in a previous paper [18].

The pH and electrical conductivity (EC) of the biochars were measured in the biochar suspension, which was formed by dispersing 1.0 g of biochar powder into 10.0 ml of distilled water. The pH value was measured using a pH meter (Mettler Toledo FiveEasy F20) and the EC value was measured by a multi-parameter meter (Portable Conductivity, Salinity and Temperature Instrument VWR CO310).

N_2 adsorption–desorption isotherms were recorded on a Micrometrics ASAP 2020 analyzer. The specific surface area and porosity of the biochars were then determined via the Brunauer Emmett-Teller (BET) method. Before the measurement, biochar samples were degassed at 300 °C under vacuum for 3 h to eliminate adsorbed species. The surface functional groups on the biochars were qualitatively analyzed using a Fourier transform infrared spectrometer (FTIR, Nicolet 5700, USA). The X-ray diffraction (XRD) patterns of the biochars were obtained at room temperature using a PANalytical X'Pert PRO diffractometer with Cu-Kα radiation. The Bragg angle (2θ) was scanned between 5° and 70° with a speed of 0.05°/min and a step size of 0.017°. The X-ray photoelectron spectra (XPS) were recorded using a Thermo ESCALAB 250Xi with Al Kα radiation as the X-ray source. Binding energies were calibrated against the C 1 s peak at 284.4 ± 0.2 eV.

2.4. Microbial analysis

The structure of the microbial community in different groups was analyzed by the high-throughput 16S rRNA gene sequencing. Samples for microbial analysis were taken from the original inoculum, the effluent in the control group G0, and the effluents in the biochar amended groups G1 to G3. The DNA extraction and further processing to identify the bacteria and archaea communities were performed by Shanghai Majorbio Biopharm Technology Co., Ltd (Shanghai, China). The methods for sample preparation and microbial analysis were detailed in a previous paper [35]. The sequence data were analyzed on the Majorbio Cloud Platform (www.majorbio.com). Operational taxonomic units (OTUs) were defined as a set of sequences clustered at 97% similarity. OTUs were taxonomically classified using RDP Classifier with reference to the RDP database. The raw sequence data were deposited into the Sequence Read Archive database of the National Center for Biotechnology Information (NCBI) with a BioProject accession code of PRJNA691752.

2.5. Kinetic calculation

The process kinetic parameters including the maximum biomethane yield (H_m), peak biomethane production rate (R_m), and lag-phase time (λ) were calculated by fitting the modified Gompertz Equation (Eq. (1)):

$$H = H_m \times \exp\left\{-\exp\left[\frac{R_m e}{H_m}(\lambda - t) + 1\right]\right\} \quad (1)$$

$$T_m = \frac{H_m}{R_m e} + \lambda \quad (2)$$

The peak time of the digestion process (T_m) was calculated as per Eq. (2). The biodegradability index (BI) was defined as the ratio of specific biomethane yield in the biomethane potential assay to the maximum theoretical biomethane potential. The maximum theoretical biomethane potential was estimated according to the Buswell Equation as expressed in Eq. (3) [36].

$$C_aH_bO_cN_d + \left(a - \frac{b}{4} - \frac{c}{2} + \frac{3}{4}d\right)H_2O \rightarrow \left(\frac{a}{2} + \frac{b}{8} - \frac{c}{4} - \frac{3}{8}d\right)CH_4 + \left(\frac{a}{2} - \frac{b}{8} + \frac{c}{4} + \frac{3}{8}d\right)CO_2 + dNH_3 \quad (3)$$

3. Results and discussion

3.1. Biochar yield, elemental composition, and surface area

The biochar yield was defined as the mass ratio of obtained biochar to the TS in the draff feedstock. Fig. 1 shows the biochar yield at different temperatures. As pyrolysis temperature increased, the biochar

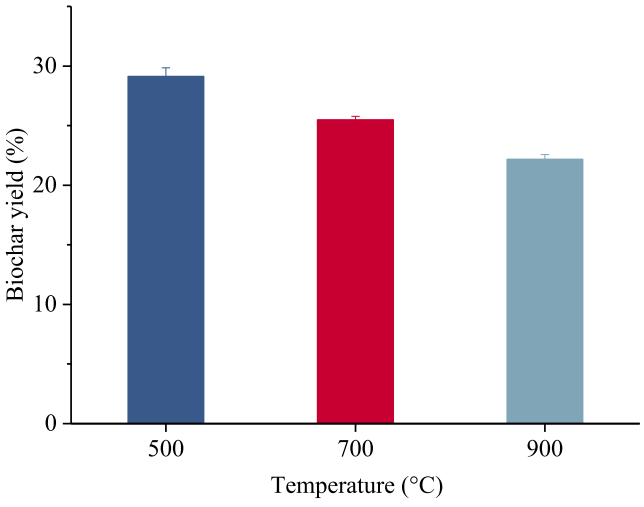

Fig. 1. The mass yield of biochar from draff at different pyrolysis temperatures.

Table 3
Compositional characteristics of the biochars.

Sample name	Elemental analysis (%TS) C	H	N	O	Ash (% TS)	HHV (MJ/kg)	Molar ratio O/C	H/C
Char_500	67.1 ± 0.2	2.1 ± 0.0	7.0 ± 0.2	11.6 ± 0.3	12.3 ± 0.8	23.7	0.13	0.37
Char_700	72.3 ± 0.5	1.1 ± 0.0	5.5 ± 0.1	6.7 ± 0.4	14.5 ± 0.3	24.9	0.07	0.19
Char_900	75.4 ± 0.7	0.7 ± 0.0	3.9 ± 0.1	5.2 ± 0.8	14.8 ± 1.1	25.5	0.05	0.11

Note: HHV = higher heating value.

yield decreased from 29.1% at 500 °C to 22.2% at 900 °C due to the loss of more volatile components. The proximate and ultimate analyses of biochars are shown in Table 3. As the temperature increased, the hydrogen, nitrogen, and oxygen content in biochars decreased. The carbon and ash content increased consequently, leading to the gradual decrease in the molar O/C (oxygen to carbon) and H/C (hydrogen to carbon) ratios. The molar ratios of O/C and H/C are important indicators to assess the degree of carbonization. The decreasing trend of H/C and O/C ratios indicated improved carbonization in the biochars as the temperature increased. Consequently, the HHV of biochars increased as the pyrolysis temperature increased.

The surface physical properties of biochars are shown in Table 4. The specific surface area of draff was as low as 0.44 m^2/g and mainly ascribed to mesopores (pores with diameters between 2 and 50 nm). At a lower temperature of 500 °C, the specific surface area increased significantly to 94.12 m^2/g and the average pore width reduced to 2.397 nm as compared to draff. The volume of micropores (pores with diameters less than 2 nm) on Char_500 contributed to 70% of the volume of total pores. As the temperature increased, the specific surface area of Char_700 increased by 142% and that of Char_900 increased by 291% as compared to Char_500. The volume of micropores increased by 162% for Char_700 and by 290% for Char_900 as compared to Char_500. The proportion of micropores (V_{micro}/V_{total}) increased to 70%, 81% and 72% for Char_500, Char_700 and Char_900, respectively as compared to 0% for Draff. Yin et al. ascribed the higher adsorption capacity of biochar to higher specific surface area and higher porosity [37]. However, other studies suggested that the specific surface area might not predominate over the adsorption behavior [38]. For example, the surface functional groups (such as acidic functional groups or hydrogen bonding) and the cationic exchange capacity might play the primary role in determining the adsorption capability [15]. Even if the interactions between the surface functional groups and the absorbate might play a role in the adsorption, higher specific surface area and porosity are key parameters to enhance the adsorption capacity of biochars.

The pH values for these biochars ranged from 7.67 to 6.99 and decreased with the increase in pyrolysis temperature. These pH values were lower compared to the pH value of 8.95–9.22 for the woody biochar previously studied [18], suggesting a lower buffering capacity of draff-derived biochars. The conductivity values of Char_500 and Char_700 exhibited no significant difference but the conductivity of Char_900 was 49% higher as compared to Char_700. The conductivity of biochar suspension was impacted by the bulk conductivity of solid biochar and the ion exchanging capacity of biochar. The improvement in conductivity suggested that Char_900 exhibited the highest capacity for transferring electrons in a suspension without engagement in microbial metabolism. These results suggested that Char_700 and Char_900 might be preferable over Char_500 for addition in AD due to the higher specific surface area, higher porosity, and high conductivity in the suspension.

Table 4
Surface properties, pH, and EC of biochars.

Sample name	S_{BET} (m^2/g)	V_{total} (cm^3/g)	V_{micro} (cm^3/g)	Avg. pore width (nm)	pH	EC (μS/cm)
Char_500	94.12	0.056	0.039	2.397	7.67 ± 0.01	207.0 ± 3.2
Char_700	227.78	0.126	0.102	2.207	7.12 ± 0.02	202.8 ± 2.5
Char_900	368.10	0.209	0.152	2.272	6.99 ± 0.00	302.9 ± 1.9
Draff	0.44	0.001	0.000	7.124		\

Note: S_{BET} = specific surface area, V_{total} = volume of total pores, V_{micro} = volume of micropores, EC = electricity conductivity.

3.2. Effects of biochar addition on anaerobic digestion

3.2.1. Effects on biomethane production

In addition to the utilization as feedstock for biochar production, draff is also suitable for biogas production in AD. The biomethane yield from draff is shown in Fig. 2 as portrayed by the biomethane potential assay. In the control group G0, the biomethane yield was 302.3 ml/g VS and the BI was 58.4%. The three different biochars showed different effects on biomethane yield. Char_500 significantly ($p < 0.05$) inhibited the biomethane yield by 12%, leading to a decreased BI of 51.6%.

This might result from an excessive dosage of Char_500 causing inhibition to AD or the relatively low quality of Char_500. Similarly, a 37% reduction in biomethane yield caused by walnut shell biochar in the co-digestion of food waste and sludge was observed (Table 1), which was ascribed to the high concentration of mono- and di-valent cations released from the biochar into the digester [31]. Char_700 statistically ($p < 0.05$) increased biomethane yield by 5% compared to the yield in G0. Char_900 did not significantly ($p > 0.05$) change the biomethane yield compared to G0. Table 5 shows the kinetic parameters calculated according to the modified Gompertz Equation. The peak production rate in Char_500 amended group decreased by 7% compared to that in G0. Unlike their distinct effects on biomethane yield, Char_700 and Char_900 slightly ($p > 0.05$) enhanced the peak production rate by 1% and 4%, respectively. Similar values of lag-phase time were observed in all the control and biochar amended groups.

3.2.2. Profiles of volatile fatty acids

The variation of VFAs during the digestion process is shown in Fig. 3. For all groups, the total VFAs accumulation reached the peak value on day 6 and then began to decrease till the end of the process. The highest

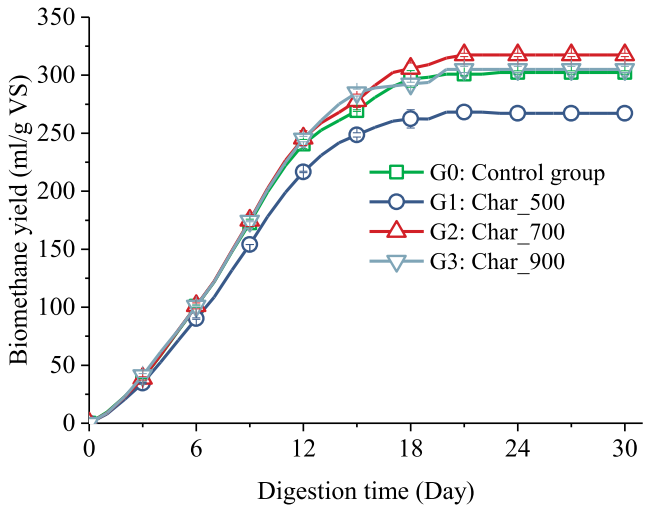

Fig. 2. The biomethane yield in the digestion of draff with the addition of different biochars.

Table 5
Kinetic parameters for the digestion of draff with different biochars.

Group	Experimental Results				Kinetic model parameters				
	BMP (ml/g VS)	BI (%)	Initial pH	End pH	H_m (ml/g VS)	R_m (ml/g VS /d)	λ (d)	T_m (d)	R^2
G0: Control	302.3 ± 1.4	58.4	8.06 ± 0.00	7.89 ± 0.06	308.4 ± 1.5	26.8 ± 0.5	2.2 ± 0.1	6.4 ± 0.1	0.998
G1: Char_500	267.2 ± 5.6	51.6	8.05 ± 0.01	7.92 ± 0.06	273.0 ± 1.7	24.8 ± 0.7	2.3 ± 0.1	6.3 ± 0.1	0.997
G2: Char_700	317.4 ± 1.4	61.3	8.03 ± 0.01	7.91 ± 0.02	324.4 ± 1.6	27.2 ± 0.5	2.2 ± 0.1	6.6 ± 0.1	0.998
G3: Char_900	305.1 ± 2.7	58.9	8.04 ± 0.01	7.91 ± 0.01	310.9 ± 2.0	27.8 ± 0.7	2.3 ± 0.2	6.4 ± 0.1	0.997

Note: BMP = biomethane potential, BI = biodegradability index, H_m = maximum biomethane yield, R_m = peak biomethane production rate, λ = lag-phase time, and T_m = peak time of the digestion process.

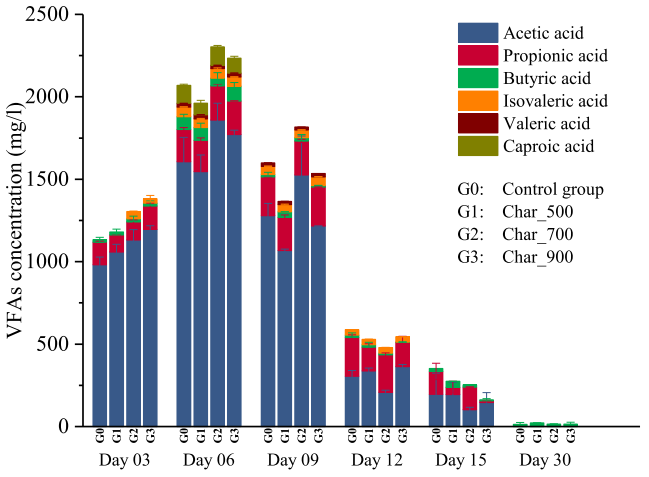

Fig. 3. The VFAs accumulation in different groups during the digestion of draff.

concentration of total VFAs for the control group G0 was 2068.6 mg/L, of which acetic acid, propionic acid, and butyric acid represented 77.7%, 9.4%, and 3.7%, respectively. On day 9, the concentration of acetic acid in G0 decreased by 20% compared to the peak value on day 6 due to the action of acetoclastic methanogenesis. The concentration of butyric acid decreased by 81% on day 9 compared to the peak value on day 6. No significant change in propionic acid concentration was observed between day 6 and 9. On day 12, the acetic acid reduced by 81.0% compared to the peak value on day 6, while the degradation of propionic acid did not take place yet at this stage. At the end of the process, the VFAs were almost completely degraded with a small amount of butyric acid remaining.

In the Char_500 amended group G1, the total VFAs reached the highest concentration of 1961.1 mg/l on day 6, presenting a 5% decrease compared to that in G0. On day 12, 78.0% of acetic acid was consumed compared to the peak value on day 6. The production and degradation efficiency of acetic acid during the first twelve days in G1 was the lowest among the four groups.

In the Char_700 amended group G2, the highest concentration of total VFAs reached 2303.0 mg/l on day 6, 11% higher than that in G0. The composition of total VFAs also changed: the share of acetic acid increased to 80.7% and the share of propionic and butyric acids were 9.0% and 2.0%, respectively. On day 12, the concentration of acetic acid decreased by 88% compared to the peak value on day 6.

In the Char_900 amended group G3, the highest VFAs concentration on day 6 was 2234.2 mg/l, in which acetic acid accounted for 79.3%. On day 9, both the concentration and composition of the total VFAs were close to those in G0. On day 12, the concentration of acetic acid decreased by 79.5% compared to the peak value. G3 was not distinct from G0 in terms of the VFAs concentration and composition. The final pH values of the effluents ranged from 7.89 to 7.92 (see Table 5) for all the control and biochar amended groups, which were all in the optimal pH range.

3.2.3. Microbial community structure

The classification of the bacteria and archaea communities is shown in Fig. 4. The bacteria community in all the groups were dominated by *Firmicutes* (60.9 – 67.5%) at the phylum level, accompanied by *Bacteroidetes* (3.3 – 5.8%), *Proteobacteria* (0.7 – 2.3%), *Atribacteria* (0.7 – 3.1%), and *Synergistetes* (0.6–3.7%) as shown in Fig. 4 (a). Compared to the original inoculum, the relative abundance of *Firmicutes* in the control group increased from 63.4% to 67.0%. Compared to the control group, the relative abundance of *Firmicutes* in Char_500 group (60.9%) and Char_900 group (61.0%) were both lower; in contrast, the relative abundance of *Firmicutes* in Char_700 group was slightly improved to 67.7%. *Firmicutes* contain acidogenic and acetogenic bacteria which convert various organic matters to VFAs and subsequently to acetate, H_2, and CO_2. The enrichment in *Firmicutes* indicated the acclimatization of the inoculum which facilitated the biomethane production from draff. *Clostridiales* was the major stream in *Firmicutes*. Representatives in *Clostridiales* such as *Ruminococcaceae* and *Clostridiaceae* are hydrolytic and acidogenic bacteria and shown to be electroactive [22,39]. Other bacteria that were highly enriched in the presence of Char_700 were *Bacteroidetes*. The relative abundance of *Bacteroidetes* in the control group was 3.3% and it increased to 4.7% in the Char_500 group, 5.8% in the Char_700 group, and 4.2% in the Char_900 group. Strains in *Bacteroidetes* play a crucial role in the decomposition of organic matters by secreting various hydrolyzing enzymes [40]. The enrichment in *Bacteroidetes* could benefit the digestion of draff.

Five archaea genera, *Methanoculleus*, *Methanobrevibacter*, *Methanosarcina*, *Methanobacterium*, and *Methanosphaera*, were predominant in the archaea community for all the groups as shown in Fig. 4 (b). Compared to the control group, the relative abundance of *Methanosarcina* significantly increased from 20.0 % to 24.9% in the Char_700 group, to 27.8% in the Char_900 group, but decreased to 17.6% in the Char_500 group. *Methanosarcina* contains both acetoclastic and hydrogenotrophic species that can convert various substrates such as acetate, methanol, and H_2/CO_2 to biomethane. *Methanosarcina* has been proven to establish DIET with *Geobacter* [41–43]. They prefer to accept electrons through DIET to produce biomethane when conductive carbon materials are introduced into the system [43–45]. Previous studies found that *Methanosarcina* instead of *Methanosaeta* was the dominant archaea in the biochar amended digester [46,47]. The enrichment of *Methanosarcina* in the Char_700 group might indicate the enhanced DIET by Char_700, resulting in the increase in biomethane yield. The abundance of *Methanoculleus* in the Char_700 and Char_900 groups also increased. *Methanoculleus* are hydrogenotrophic and cannot directly use acetic acid to produce biomethane [22]. In contrast, the abundance of *Methanobrevibacter*, *Methanobacterium* and *Methanosphaera* decreased in the Char_700 and Char_900 groups but increased in the Char_500 group. *Methanobrevibacter* and *Methanobacterium* are typical H_2 utilising methanogens. The decrease in the abundance of *Methanobrevibacter* and *Methanobacterium* suggested the possible shift of the interspecies electron transfer pathway from the MIET mode to the DIET mode. Interestingly, Shen et al. found a significant negative correlation between biochar's electron-accepting capacity and the abundance of hydrogenotrophic

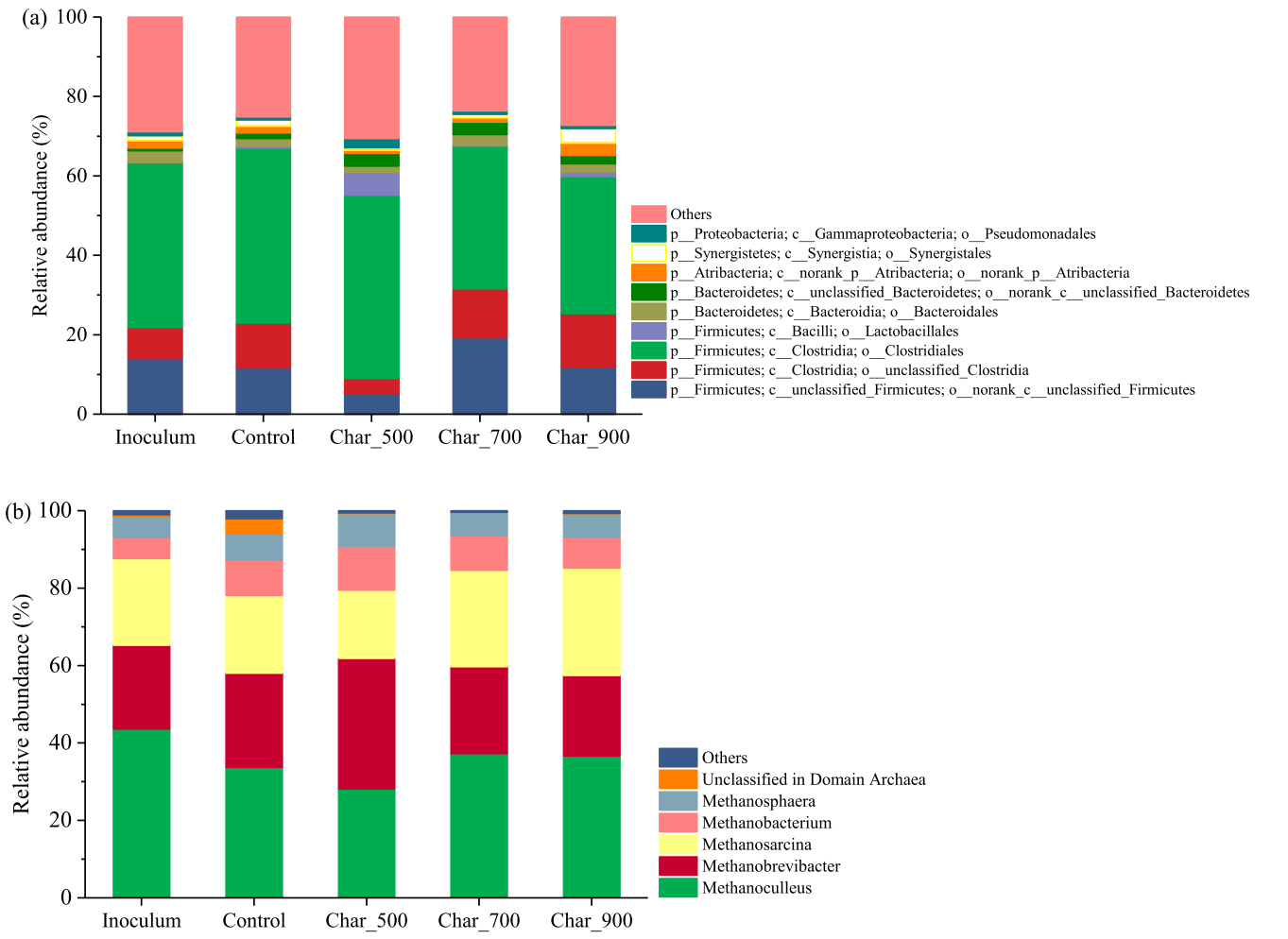

Fig. 4. Classification of (a) bacteria community at the Order level and (b) archaea community at the Genus level. Species with relative abundance less than 2% were classified in others.

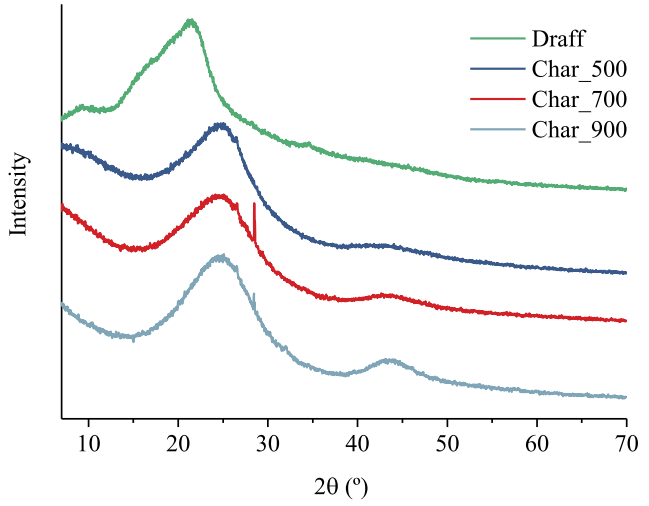

Fig. 5. The XRD spectra of draff and biochars derived at different pyrolysis temperatures.

Methanobacterium and a significant negative correlation between biochar's electron-donating capacity and the abundance of H_2-dependent methylotrophic *Methanosphaera* [21].

3.3. Chemical properties of biochar

3.3.1. X-ray diffraction results

Fig. 5 shows the crystalline properties of biochars identified by the XRD spectra. The broad peak centered at the 2θ value of 22° for the draff sample was assigned to the crystalline region of cellulose [48]. In biochar samples, the broad peak for crystalline cellulose disappeared, indicating the decomposition of cellulose during pyrolysis. A broad and strong peak centered at 24° in biochar samples was the (002) peak of turbostratic carbon [49]. Another peak at 44° observed in biochars was contributed by the (10) peak of graphite [50]. The 44° peak in Char_500 was unobservable. The intensity of 44° peak in Char_700 and Char_900 increased as the pyrolysis temperature increased, indicating the formation of more graphitic structures at higher pyrolysis temperatures. The graphitization degree in the biochars was compared through the measurements of apparent interlayer spacing (d_{002}) and microcrystallite diameter (L_a). The interlayer spacing (d_{002}) indicated the packing density of carbon layers and was estimated by the Bragg's law $n\lambda = 2d_{002}\sin\theta$ (n = 2) [51]. The microcrystallite diameter L_a was estimated according to the Warren's formula (Eq.4) [52].

$$L_a = \frac{1.84\lambda}{B\cos\theta} \tag{4}$$

where λ is the X-ray wavelength (0.154 nm), θ is the Bragg angle, and B is the line broadening at half the maximum intensity in radian. The average spacing d_{002} was about 0.37 nm for all the biochars, slightly

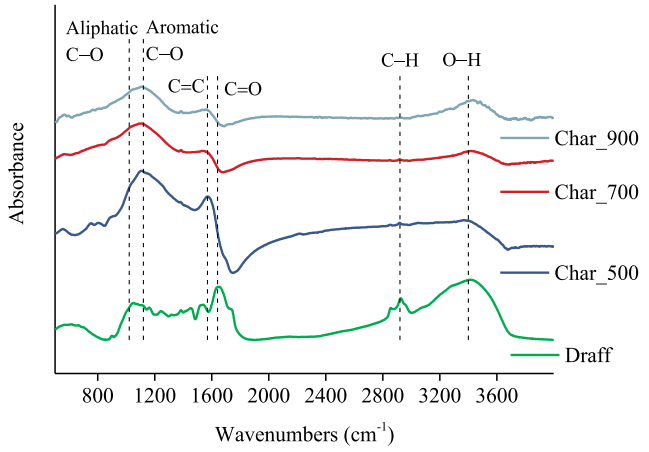

Fig. 6. The FTIR analysis of draff and biochars derived at different pyrolysis temperatures.

larger than the d_{002} of 0.34 nm for graphite [52]. The pyrolysis temperature imposed little influence on d_{002}. The microcrystallite diameter L_a increased in biochars as the temperature increased. The L_a for Char_500, Char_700, and Char_900 was 1.34, 1.91, and 3.71 nm, respectively. The increase in L_a indicated the lateral growth of the graphitic carbon layer in the carbonization process.

3.3.2. *Fourier transform infrared spectroscopy results*

Fig. 6 shows the FTIR spectra of draff and biochars. The absorbance peak at around 3400 cm^{-1} was attributed to the stretching of O–H [53]. The absorbance peak at 2930 cm^{-1} was due to the stretching of aliphatic C–H [53]. The peak at 1640 to 1650 cm^{-1} was due to the stretching of quinone/ketone C═O [54,55]. The intensive O–H, C–H, and C═O peaks were flattened or disappeared as the pyrolysis temperature increased due to the breakage of the functional groups by the dehydroxylation, decarboxylation, decarbonylation, and demethoxy reactions. The peak at 1570 cm^{-1} observed only with biochar samples was due to the stretching vibration of aromatic C═C [54]. The peaks at 1120 and 1020 cm^{-1} were attributed to the stretching vibration of aromatic C–O and aliphatic C–O, respectively [53]. In biochar samples, the aromatic C–O peak appeared, while the aliphatic C–O peak disappeared. The occurrence of intensive C═C and aromatic C–O peaks suggested that polyaromatic structure was formed [50].

3.3.3. *X-ray photoelectron spectroscopy results*

The XPS spectra of C1s in Fig. 7 reveal the chemical status of carbon on the surface of biochars. The C1s spectra were deconvoluted into six peaks representing six functional groups: sp^2 C hybridisation peak (graphitic/aromatic carbon) at the binding energy of 284.4 eV, sp^3 C hybridisation peak (hydrocarbon) at 284.8 eV, –C–O peak (alcohol/ether) at 285.7 eV, –C═O peak (quinone/ketone) at 287.0 eV, –COOR peak (carboxyl/ester) at 288.9 eV, and the π-π* shake-up satellite peak (satellite of graphitic carbon) at 290.4 eV [56–58]. The peak area represented the relative abundance of each functional group. Normalization was conducted on the integral area of the peaks and the results are shown in Table 6. The major functional groups on draff were sp^3 C, –C–O, and –C═O groups, accounting for 84.1% of the total carbon species. The percentage of total oxygen-containing functional groups (namely –C–O, –C═O, and –COOR) on draff was 50.1%. A considerable decrease in total oxygen-containing functional groups and an increase in sp^3 C were observed on Char_500 as compared to draff due to the carbonization reactions. The relative abundance of sp^2 C on Char_700 doubled as compared to Char_500, indicating the enhanced aromatization. The increase in sp^2 C on Char_700 was accompanied by a decrease in sp^3 C. The percentage of π-π* shake-up satellite on Char_700 did not change significantly compared with Char_500. The percentage of total oxygen-containing functional groups on Char_700 slightly increased to 37.8% as compared to 32.2% on Char_500. Particularly, the percentage of –C═O doubled on Char_700 compared to Char_500. As the temperature increased to 900 °C, the percentage of sp^2 C increased to 29.5% and exceeded that of sp^3 C. The percentage of π-π* shake-up satellite reached the highest level of 13.6% on Char_900, indicating the formation of more graphitic carbon. The conjugated π-electron systems associated with condensed graphitic carbon are responsible for the bulk electrical conductivity of biochars [52,59]. The increase in sp^2 C abundance along with the increase in π-π* shake-up satellite could lead to a higher bulk electrical conductivity of Char_900 and facilitate the direct electron transfer through carbon matrices [52,60]. The percentage of oxygen-containing functional groups on Char_900 decreased to the lowest level of 29.4%. The oxygen-containing functional groups such as the quinone – hydroquinone pairs are responsible for the electron-accepting and donating capacity of biochars [21]. Char_700 had the highest percentage of 8.7% for –C═O, followed by the percentage of 8.1% for Char_900. The high abundance of –C═O on Char_700 could contribute to its capacity of electron transfer through surface charging – discharging cycles.

The deconvolution of N1s spectra in Fig. 7 revealed that pyridinic-N (6 member N heterocycles) at 398.1 eV, pyrrolic-N (5 member N heterocycle) at 399.1 – 400.0 eV, and graphitic-N at 401.2 eV were the main forms of nitrogen on biochar surface [61]. The normalized results are displayed in Table 7. Pyrrolic-N was the predominant group on draff and all the biochars. At lower temperatures, pyridinic-N formed on biochars by the conversion of thermally unstable pyrrolic-N. The relative abundance of pyridinic-N on Char_700 was higher than those on Char_500 and Char_900. At 700 and 900 °C, more pyrrolic-N was further transformed to graphitic-N. Char_700 also presented the highest abundance of graphitic-N. Both pyridinic-N and graphitic-N can donate electrons to the conductive π-system in carbonaceous materials and enhance the conductivity [62]. The electrochemical behaviour of Char_700 may be better due to its moderate nitrogen content and the highest abundance of functional pyridinic-N and graphitic-N.

3.4. *Correlations between biochar properties and facilitating effects in anaerobic digestion*

The properties of biochar determine its role in facilitating biomethane production in AD. The pyrolysis temperature as a major parameter in biochar production plays an important role in shaping the properties of biochar. Fig. 8 shows the increase in biomethane yield affected by the addition of biochars produced at different temperatures [18,21,22,26–32,39,40,44,46,63–71]. Most of the studied biochars can enhance biomethane yield by 0–50% regardless of the biomass resources and pyrolysis conditions for biochar production. However, considerable outliers exist which lead to neutral or even negative effects on biomethane yield. The 26 types of biochars produced at low temperatures (≤ 500 °C) lead to a median increase of 13% in biomethane yield within a variation range between −12% and 52%. The 25 types of biochars produced at medium temperatures (500 – 700 °C) lead to a similar median increase of 13% in biomethane yield within a smaller variation range of 0 – 37%. The 7 types of biochars produced at high temperatures (>700 °C) lead to a median increase of 3% within a variation range between −73% and 78%.

To establish relationships between the observed enhancement in AD and the properties of biochars, mathematic correlations between the increase in biomethane yield and the major properties of biochars were analyzed.

Generally, increasing pyrolysis temperature leads to higher porosity and specific surface area of biochars. Qin et al. suggested that the specific surface area was one of the key biochar properties for enhancing AD as a high specific surface area could facilitate the attachment of microorganisms and the contact between microorganisms and the available substrates [22]. Zhang et al. found that the proportion of the

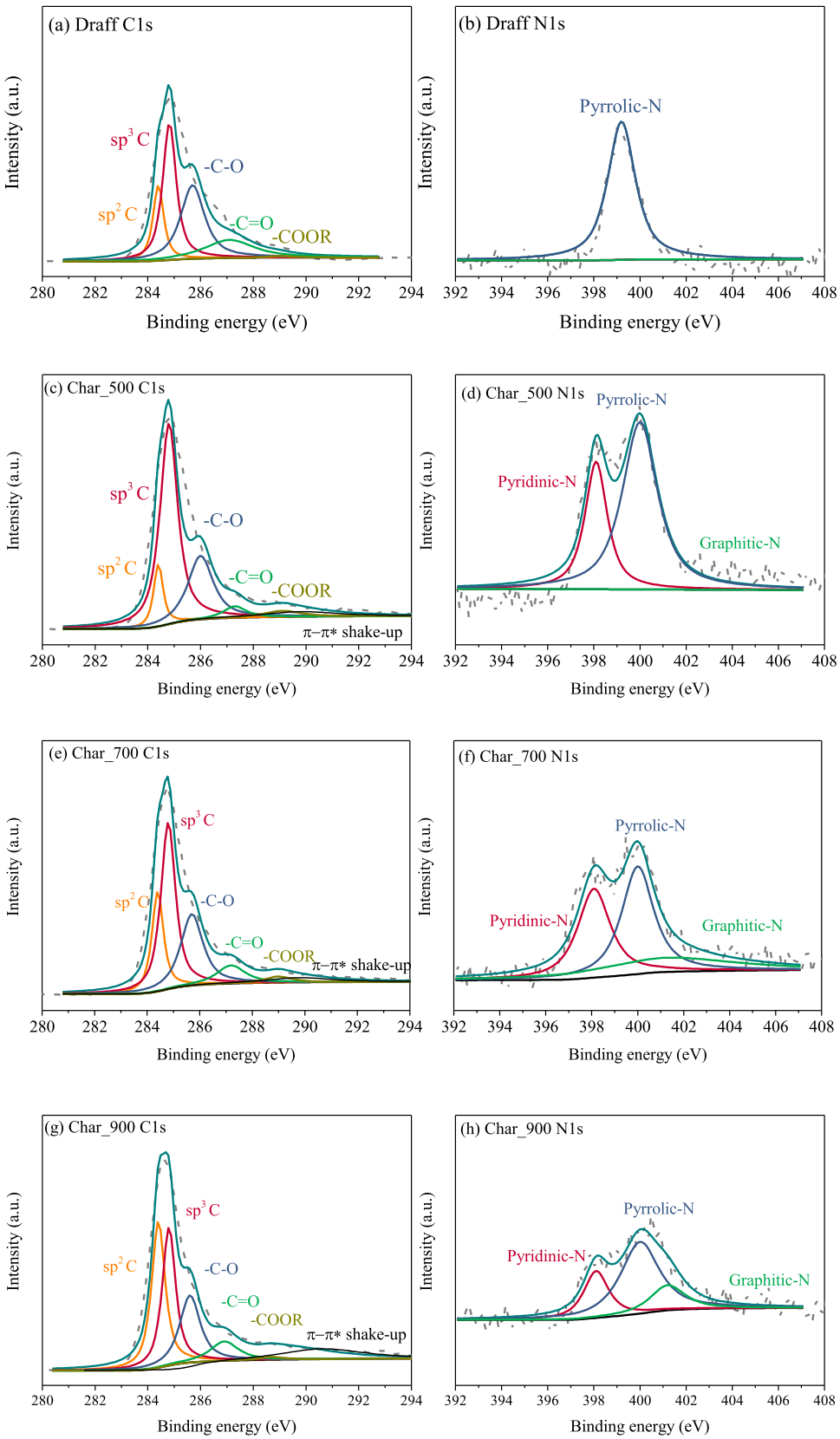

Fig. 7. The X-ray photoelectron spectra of C1s on (a) draff, (c) Char_500, (e) Char_700, and (g) Char_900; XPS spectra of N1s on (b) draff, (d) Char_500, (f) Char_700, and (h) Char_900.

Table 6
Relative abundance of different carbon functional groups.

C speciesSample	sp^2 C	sp^3 C	–C–O	–C═O	–COOR	π-π* shake-up satellite
	284.4 eV	284.8 eV	285.7 eV	287.0 eV	288.9 eV	290.4 eV
Draff	15.2%	34.7%	32.9%	16.5%	0.7%	0
Char_500	9.1%	53.8%	24.1%	4.3%	3.8%	4.9%
Char_700	19.1%	38.5%	25.7%	8.7%	3.4%	4.6%
Char_900	29.5%	27.5%	20.4%	8.1%	0.9%	13.6%

Note: The relative abundance of each functional group was determined by the integral area of the characteristic peak in the X-ray photoelectron spectra.

Table 7
Relative abundance of different nitrogen-containing functional groups.

N speciesSample	Pyridinic-N	Pyrrolic-N	Graphitic-N
	398.1 eV	399.1–400.0 eV	401.2 eV
Draff	0	100%	0
Char_500	32.7%	67.3%	0
Char_700	34.8%	41.4%	23.8%
Char_900	24.5%	57.4%	18.1%

Note: The relative abundance of each functional group was determined by the integral area of the characteristic peak in the X-ray photoelectron spectra.

microbial cells attaching to the biochar surface increased as the pyrolysis temperature increased from 700 to 900 °C due to the enlarged specific surface area and porosity [65]. It could be inferred that the higher specific surface area and higher porosity of Char_700 and Char_900 were beneficial to the attachment of microorganisms on biochar and the microbial electron transfer. However, no direct linear correlation (R^2 = −0.085) between the enhancement in biomethane yield and the specific surface area was observed as shown in Fig. 9 (a).

Higher pyrolysis temperatures generally lead to lower molar H/C and O/C ratios due to the loss of hydrogen and oxygen components. The significant decrease in H/C and O/C ratios indicated the increase in carbonization degree of Char_700 and Char_900, which was confirmed by the XRD and XPS results. In agreement with the results in this study, Zhang et al. observed that a higher conductivity of biochar was associated with a lower oxygen content [65]. The graphitic and aromatic carbon matrices in biochars are capable of directly transferring electrons and may have a significant influence on facilitating DIET in AD. For instance, the direct electron transfer through carbon matrices contributed to 87–100% of the total electron transfer by biochars derived at high temperatures (650 – 800 °C) [52]. Biochars with a molar H/C ratio lower than 0.35 and a molar O/C ratio lower than 0.09 are capable of directly transferring electrons through carbon matrices more than three times faster than the surface charging – discharging cycles [60]. The findings suggested that the electron transfer through Char_700 and Char_900 highly depended on the conductivity of carbon matrices. However, there was no linear correlation (R^2 = −0.923) between the increase in biomethane yield and the electrical conductivity (measured in the biochar suspensions) of biochars in this study as shown in Fig. 9 (b). Some researchers have also reported that the conductivity of biochars did not linearly correlate with the enhancing effect of biochar in AD [69,72].

Besides carbon matrices, the redox cycling of surface functional groups is another important mechanism for electron transfer by biochars, particularly for biochars produced at low temperatures. According to Sun et al., the redox cycling of functional groups accounted for 78 – 100% of the total electron transfer by biochars derived at 400–500 °C [52]. When applied in AD, biochars with abundant functional groups can function as an electron shuttle involving in the electron-donating/accepting cycle, thereby promoting microbial electron transfer and subsequent biomethane production [21,47]. The quinone – hydroquinone pair has been identified as the most common couple that contributes to the redox activity of biochar [21]. In this study, the relative abundance of oxygen-containing functional groups (especially –C═O groups which include quinone groups) increased as the temperature increased to 700 °C but decreased as the temperature increased further to 900 °C. Sun et al. observed the charging and discharging capacities of surface quinone groups increased from 400 to 550 °C due to the improved reactivity of quinone groups, but the capacities decreased above 550 °C due to the reduced surface functionality [60]. The threshold temperature for the turning point of the redox activity of surface functional groups might vary for different biochars due to the variation in biomass resources and pyrolysis conditions [60]. In this

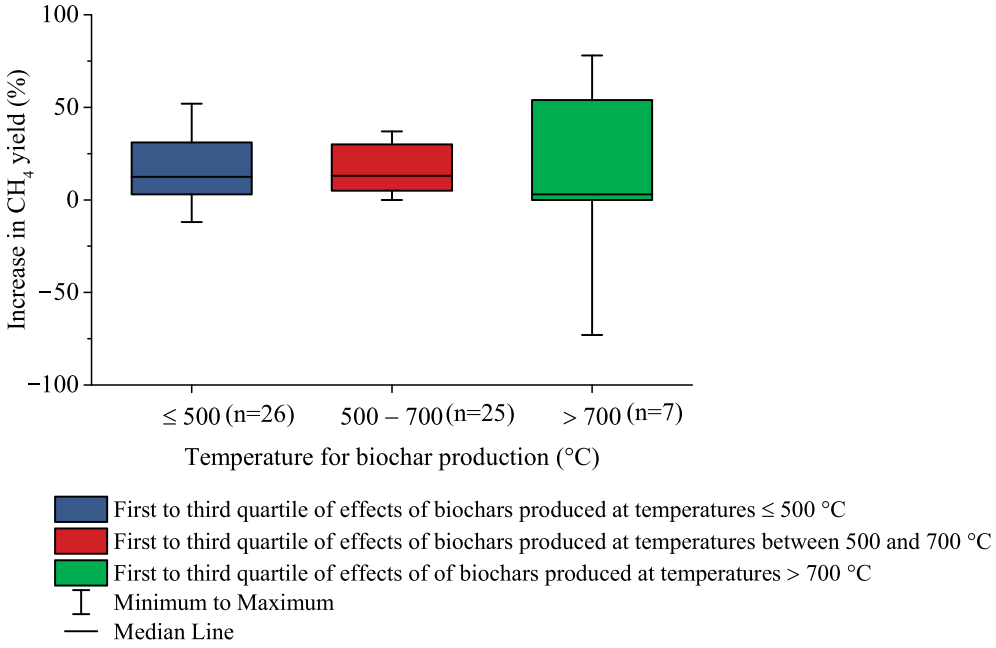

Fig. 8. The increase in biomethane yield in anaerobic digestion through the addition of biochars produced at different temperatures. The data were collected from both literature and this study [18,21,22,26–32,39,40,44,46,63–71]. Note: n = number of biochar samples.

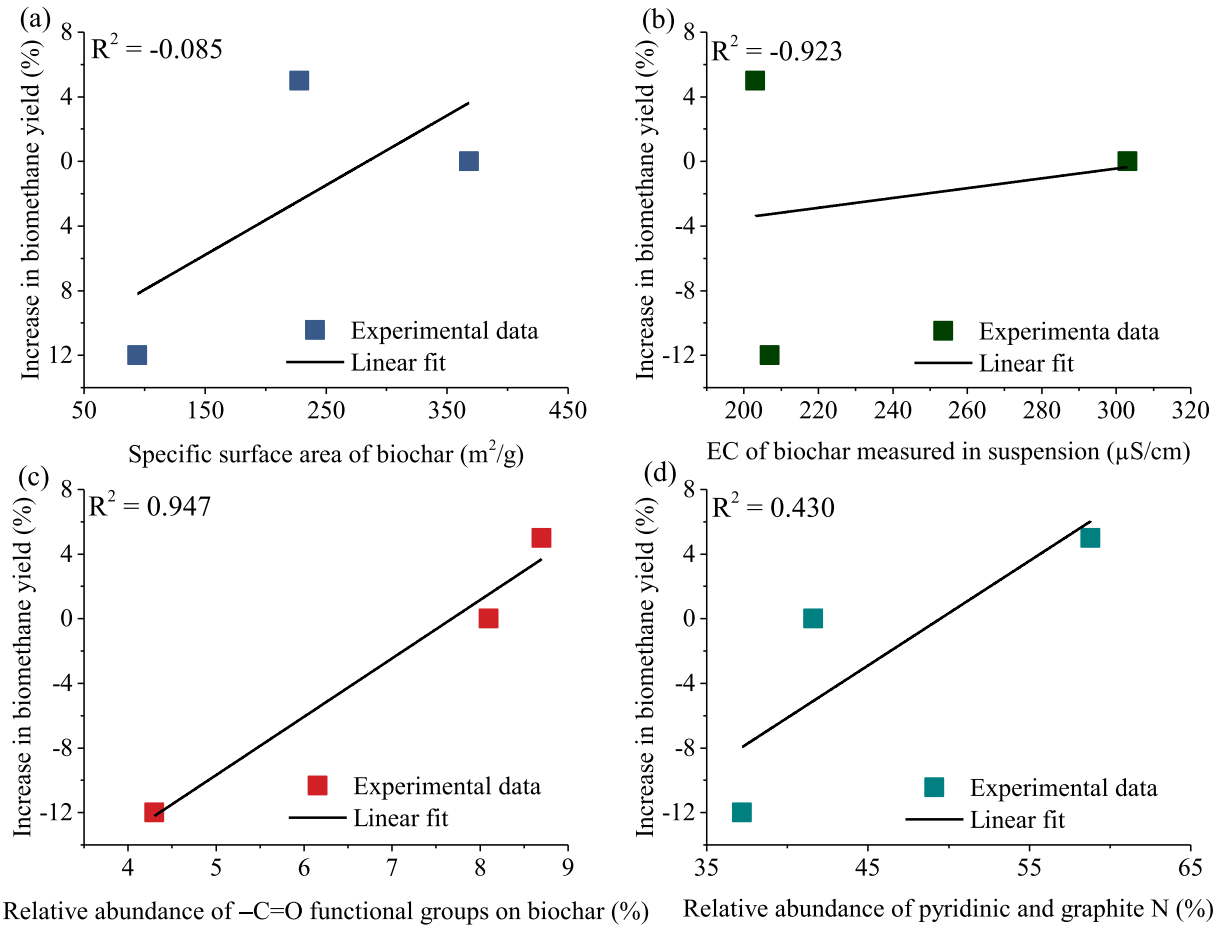

Fig. 9. Correlations between the increase in biomethane yield and the biochar properties: (a) specific surface area, (b) electrical conductivity (EC), (c) relative abundance of –C═O functional groups, and (d) relative abundance of pyridinic-N and graphitic-N.

study, a positive correlation (R^2 = 0.947) was observed between the increase in biomethane yield and the relative abundance of –C═O functional groups as shown in Fig. 9 (c). This observation suggested the –C═O groups might play an important role in enhancing AD efficiency. Further investigation of the interactions between microbes and the functional groups on biochar surface could facilitate the understanding of the fundamental drivers for biochar-stimulated interspecies electron transfer.

Although the nitrogen content in biochars was less than 10%, the surface nitrogen-containing functional groups might have significant influences on the electrochemical characteristics of biochars. The pyridinic-N and graphitic-N are both capable of donating electrons with a high reactivity [73]. The introduction of electronegative N atoms decreases the electron density of the graphite layer, which enhances the π-electron-accepting capacity of biochar [61]. The significant role of nitrogen-containing functional groups in promoting the electrochemical performance of biochars has been adequately explored [73]. Nitrogen-doped biochar derived from watermelon rind at 700 °C achieved a low charge transfer resistance comparable to that of commercial Pt/C electrodes in microbial fuel cells [74]. In this study, Char_700 had the highest abundance of pyridinic-N and graphitic-N, which might contribute to the stimulation of microbial electron transfer. However, there was only a weak positive relevance (R^2 = 0.430) between the increase in biomethane yield and the relative abundance of pyridinic-N and graphitic-N as shown in Fig. 9 (d). Nonetheless, the engagement of N-containing functional groups in the adsorption, microbial acclimation, and DIET process in the AD system has yet to be revealed.

Draff-derived biochars led to a smaller increase in biomethane yield as compared to several other biochars such as those derived from Douglas fir, soft wood, oil seed rape, canola meal, switchgrass, coconut shell, and Ashe juniper as shown in Table 1. The differences in the enhancing effects can arise from several factors such as various feedstocks, different microbial communities in the inoculum, and distinct biochar properties. The properties of biochar are important factors but not the only ones responsible for this. Char_700 exhibited a lower O content and a smaller O/C ratio compared to biochars derived from Douglas fir, soft wood, oil seed rape, canola meal, Ashe juniper, straw, and coconut shell at temperatures between 500 °C and 900 °C. It could be inferred that the smaller amount of oxygen-containing functional groups on Char_700 was associated with its lower effectiveness in enhancing biomethane yield. There were no direct correlations between the specific surface area or electrical conductivity of these biochars and the enhancement in biomethane yield. This observation was in line with the finding in this study that the –C═O groups rather than the specific surface area or the electrical conductivity might play a more significant role in facilitating biomethane production.

In this study, the biochar derived at 700 °C statistically enhanced biomethane production by 5%, which made a significant difference from the 500 °C-derived biochar. The increase in biomethane production is expected to be enlarged with future optimization of biochar properties and its addition strategy in AD. The shift of microbial structure towards the increase in *Methanosarcina* in the Char_700 amended group indicated the potential enhancement in microbial interspecies electron transfer. The proposed mechanisms for microbial electron transfer facilitated by different biochars are shown in Fig. 10. As discussed above, the higher capacity of Char_700 for facilitating microbial interspecies electron transfer was postulated as being associated with the high specific surface area, high abundance in graphitic/aromatic

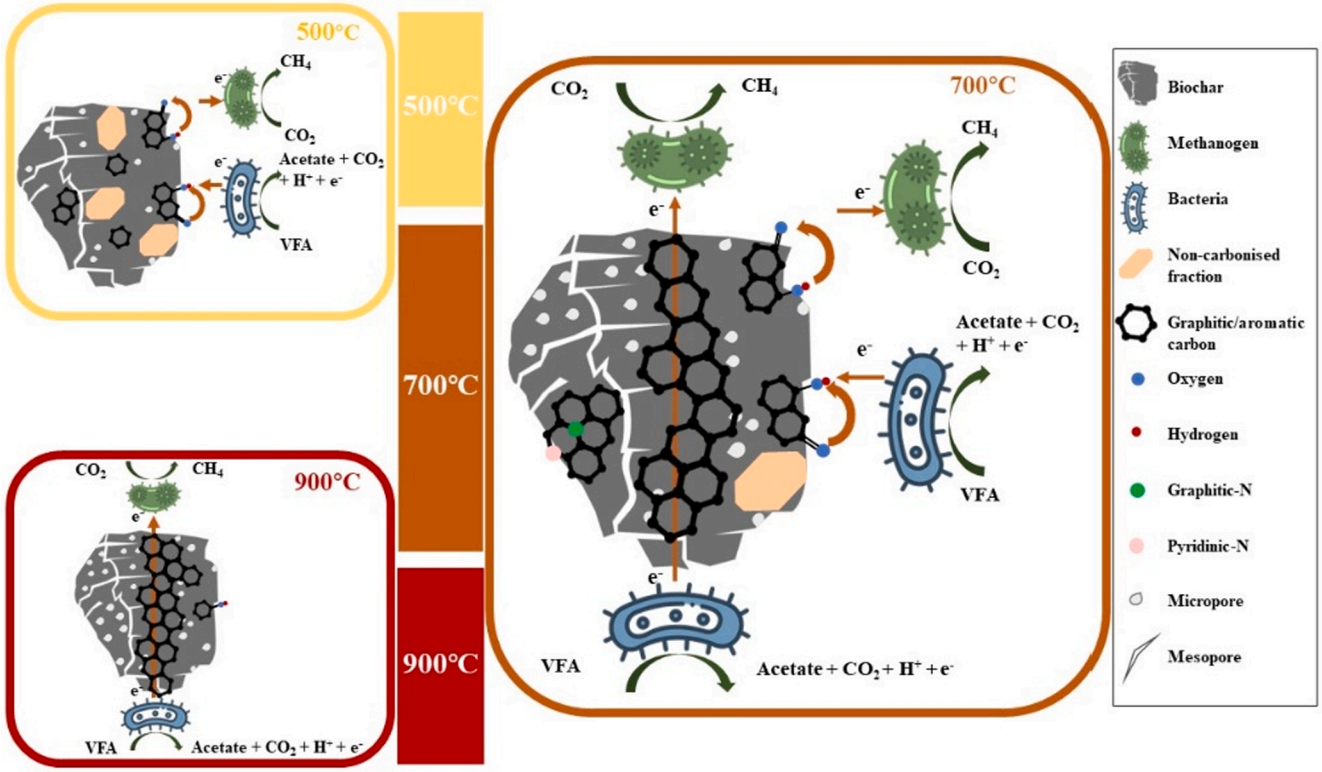

Fig. 10. The proposed mechanisms of microbial electron transfer stimulated by biochars produced at different temperatures.

carbon, abundant oxygen-containing functional groups (–C═O groups), and abundant active nitrogen-containing functional groups (pyridinic-N and graphitic-N). The higher capacity of stimulating microbial electron transfer through both carbon matrices and surface functional groups was possibly responsible for the best performance of Char_700 in enhancing biomethane yield. The Char_900 amended group presented no significant difference with the control group in biomethane production possibly due to the reduced surface functional groups. This phenomenon suggested that electrical conductivity might not be the critical factor for assessing the efficacy of biochar in promoting DIET. The electron transfer by Char_500 relied largely on the charging – discharging cycle of the surface functional groups given the low graphitization degree. However, Char_500 showed poor surface and pore properties, and a low abundance of functional groups such as –C═O, pyridinic-N, and graphitic-N, which might collectively lead to its lowest capacity in facilitating microbial electron transfer. Furthermore, the presence of Char_500 in AD might introduce adverse effects, such as the adsorption of nutrients and useful metabolites, reduced interaction amongst microorganisms, and the destruction of microorganism diversity [75–77].

3.5. Potential implementation and future perspectives

A preliminary mass and energy balance for the AD of draff and pyrolysis for biochar production was assessed. The mass and energy balance of a conventional AD system without biochar addition was calculated based on the BMP results in section 3.2.1. The calculation methods and results are presented in Table S1 in the supplementary material. Briefly, the energy output from the AD of 1.00 kg draff (wet weight) is 3.69 MJ, which is the HHV of the produced biomethane. The primary energy consumption for operating the AD process is 0.22 MJ. The net energy gain from the AD of 1.00 kg draff is 3.47 MJ. The mass and energy balance for the biochar production was estimated based on the data adapted from Aimaro et al. [78] which investigated the pyrolysis of wheat and barley spent grain. The primary process parameters adapted from Aimaro et al. [78] include (1) the yield and HHV of the produced biochar, bio-oil, and syngas, (2) the energy consumption for grinding, drying, and pyrolysis of draff, and (3) the energy used to produce the ice required for the tar-trap. Detailed calculations for the mass and energy balance of the pyrolysis are presented in Table S2 in the supplementary material. To match the AD of 1.00 kg draff (containing 0.31 kg VS), the calculations for the pyrolysis are based on the pyrolysis of 1.45 kg draff which produces 0.08 kg of biochar which satisfies the calculation of addition to the digester at a mass ratio of 25% (biochar to the VS of the feedstock in AD). As such, in addition to 0.08 kg biochar, 0.24 kg bio-oil and 0.14 kg syngas are co-produced. The energy output of the pyrolysis in terms of the energy value of the bio-oil and syngas, is 4.91 MJ. The total energy consumption of the pyrolysis process is 4.00 MJ. Therefore, the net energy gain from the individual pyrolysis of 1.45 kg draff is 0.91 MJ. When biochar is added into the digester, the net energy gain from the AD process increases by 0.19 MJ due to the 5% increase in biomethane yield. The trade-off between the cost of biochar production and the benefits of adding biochar into AD depends on the application routes of biochar:

(1) If biochar is seen as a solid fuel, the energy value of biochar is an energy loss due to the application of biochar in AD (1.95 MJ of biochar VS 0.19 MJ of the increased biomethane). An increase of at least 53% in biomethane yield is necessary to compensate for the loss of energy in this case.
(2) If biochar is seen as a soil additive to increase organic carbon in soils rather than a solid fuel [79], it has negative emission potential when applied into the soil after the application in AD. Anaerobic digestate derived from biochar-amended AD has been reported to improve agronomic qualities with improved biomass yield [38]. Therefore, the increase in biomethane yield in AD can be regarded as an extra benefit of biochar.

The optimal application of biochar in a large-scale AD system could have potential to create additional economic and environmental benefits as outlined below:

(1) Further optimization of biochar properties and additional digestion strategies could enlarge the enhancing effects of biochar on AD performance. Desirable biochar properties include for: abundant surface functional groups (particularly –C═O, pyridinic-N, and graphitic-N); increased surface area and pore volume; high electrical conductivity; and high alkalinity potential. A deeper understanding of the role of biochar in AD from the microscopic scale will help to identify the optimal range of biochar properties and facilitate the production of tailored biochar to enhance AD performance, leading to a more significant enhancement above and beyond the 5% achieved here.
(2) In addition to the increase in biomethane yield, the addition of biochar may lead to a number of other co-benefits. As demonstrated in the literature, biochar can enhance AD stability, buffer pH, support microbial growth, improve agronomic qualities of the digestate, and increase soil organic carbon when applied to land [38]. These co-benefits should all be considered when assessing the benefits of a biochar amended AD system in future studies.
(3) Further integration of the AD and pyrolysis systems will facilitate the enhancement of both economic and environmental benefits. The development of further technology integration such as biochar amended biomethanation via the biological Sabatier reaction [80] or pyrolysis of solid digestate [18] offers potential opportunities for further enhanced energy production efficiency and enabling of a zero-emission technology system [81]. The economic feasibility and environmental sustainability of such integrated systems need evidence based justification.

4. Conclusion

This study showed that biochar produced from the whiskey by-product draff at different temperatures led to distinct effects on biomethane yield in AD. The distinct effects are highly dependent on the surface chemical properties of biochars. Increasing the pyrolysis temperature from 500 to 700 °C facilitated the graphitization of the carbon fraction and enhanced the abundance and activity of surface functional groups in biochars. The 700 °C-derived biochar statistically enhanced biomethane yield by 5%. The capacity of 700 °C-derived biochar for enhancing interspecies electron transfer was postulated as being associated with a moderate graphitization degree and a high abundance of surface functional groups such as –C═O groups, pyridinic-N, and graphitic-N. A further increase in the pyrolysis temperature above 700 °C reduced the abundance of surface functional groups on biochar, which led to the decreased capacity in promoting interspecies electron transfer. Comprehensive optimization of the addition of 700 °C-derived biochar in AD is necessary to further enhance biomethane production from draff. Future studies are required to evaluate the techno-economic viability of a circular bioenergy system incorporating biochar into AD.

CRediT authorship contribution statement

Chen Deng: Conceptualization, Methodology, Investigation, Writing – original draft. **Richen Lin:** Conceptualization, Methodology, Writing - review & editing, Funding acquisition. **Xihui Kang:** Investigation, Writing - review & editing. **Benteng Wu:** Investigation, Writing - review & editing. **David M Wall:** Validation, Writing - review & editing, Funding acquisition. **Jerry D Murphy:** Conceptualization, Validation, Supervision, Funding acquisition, Writing - review & editing.

Declaration of Competing Interest

The authors declare that they have no known competing financial interests or personal relationships that could have appeared to influence the work reported in this paper.

Acknowledgements

This study was funded by Science Foundation Ireland (SFI) through the Centre for Energy, Climate, Marine (MaREI) under Grant No. 12/RC/2302_P2 and 16/SP/3829, the European Regional Development Fund under the Interreg NWE Project BioWILL (No. NWE 964), the Environmental Protection Agency – Ireland (2018-RE-MS-13), Sustainable Energy Authority Ireland (RDD/00454), and the SFI Future Innovator Prize Zero Emissions Challenge project Electrofuels in a Circular Economy (EFACE) (19/FIP/ZE/7565). Industrial co-funding from Gas Networks Ireland through the Gas Innovation Group is also gratefully acknowledged.

Appendix A. Supplementary data

Supplementary data to this article can be found online at https://doi.org/10.1016/j.fuel.2021.121736.

References

[1] Fagerström, A., Seadi, T.A. Rasi, S. Briseid. T. The role of anaerobic digestion and biogas in the circular economy. in: J.D. Murphy, (Ed.). IEA Bioenergy Task 372018.
[2] Long A, Murphy JD. Can green gas certificates allow for the accurate quantification of the energy supply and sustainability of biomethane from a range of sources for renewable heat and or transport? Renew Sustain Energy Rev 2019;115:109347.
[3] IEA. Outlook for biogas and biomethane: Prospects for organic growth World Energy Outlook Special Report. Paris: IEA; 2020.
[4] the European Commission. Directive (EU) 2018/2001 of the European Parliament and of the Council of 11 December 2018 on the promotion of the use of energy from renewable sources; 2018.
[5] the European Commission. Renewable Energy Progress Report, Report from the Commission to the European Parliament, the Council, the European Economic and Social Committee and the Committee of the Regions; 2019.
[6] Gray N, McDonagh S, O'Shea R, Smyth B, Murphy JD. Decarbonising ships, planes and trucks: An analysis of suitable low-carbon fuels for the maritime, aviation and haulage sectors. Adv Appl Energy 2021;1.
[7] O'Shea R, Lin R, Wall DM, Browne JD, Murphy JD. Using biogas to reduce natural gas consumption and greenhouse gas emissions at a large distillery. Appl Energy 2020;279.
[8] Ghysels S, Ronsse F, Dickinson D, Prins W. Production and characterization of slow pyrolysis biochar from lignin-rich digested stillage from lignocellulosic ethanol production. Biomass Bioenerg 2019;122:349–60.
[9] Buss W, Jansson S, Wurzer C, Mašek O. Synergies between BECCS and Biochar—Maximizing Carbon Sequestration Potential by Recycling Wood Ash. ACS Sustainable Chem Eng 2019;7:4204–9.
[10] Awasthi MK, Sarsaiya S, Wainaina S, Rajendran K, Awasthi SK, Liu T, et al. Techno-economics and life-cycle assessment of biological and thermochemical treatment of bio-waste. Renew Sustain Energy Rev 2021;144.
[11] Lin R, Cheng J, Ding L, Murphy JD. Improved efficiency of anaerobic digestion through direct interspecies electron transfer at mesophilic and thermophilic temperature ranges. Chem Eng J 2018;350:681–91.
[12] Lu J-S, Chang J-S, Lee D-J. Adding carbon-based materials on anaerobic digestion performance: A mini-review. Bioresour Technol 2020;300:122696. https://doi.org/10.1016/j.biortech.2019.122696.
[13] Wu Y, Wang S, Liang D, Li N. Conductive materials in anaerobic digestion: From mechanism to application. Bioresour Technol 2019;122403.
[14] Lin R, Deng C, Cheng J, Xia A, Lens PNL, Jackson SA, et al. Graphene Facilitates Biomethane Production from Protein-Derived Glycine in Anaerobic Digestion. iScience 2018;10:158–70.
[15] Chiappero M, Norouzi O, Hu M, Demichelis F, Berruti F, Maria FD, et al. Review of biochar role as additive in anaerobic digestion processes. Renew Sustain Energy Rev 2020;131:110037.
[16] Zhao Z, Li Y, Zhang Y, Lovley DR. Sparking anaerobic digestion: promoting direct interspecies electron transfer to enhance methane production. iScience 2020;23:101794.
[17] Qi Q, Sun C, Zhang J, He Y, Wah Tong Y. Internal enhancement mechanism of biochar with graphene structure in anaerobic digestion: The bioavailability of trace elements and potential direct interspecies electron transfer. Chem Eng J 2021;406:126833.
[18] Deng C, Lin R, Kang X, Wu B, O'Shea R, Murphy JD. Improving gaseous biofuel yield from seaweed through a cascading circular bioenergy system integrating anaerobic digestion and pyrolysis. Renew Sustain Energy Rev 2020;128.
[19] Feng Q, Lin Y. Integrated processes of anaerobic digestion and pyrolysis for higher bioenergy recovery from lignocellulosic biomass: A brief review. Renew Sustain Energy Rev 2017;77:1272–87.
[20] Zhou H, Brown RC, Wen Z. Biochar as an Additive in Anaerobic Digestion of Municipal Sludge: Biochar Properties and Their Effects on the Digestion Performance. ACS Sustainable Chem Eng 2020;8:6391–401.
[21] Shen Y, Yu Y, Zhang Y, Urgun-Demirtas M, Yuan H, Zhu N, et al. Role of redox-active biochar with distinctive electrochemical properties to promote methane

production in anaerobic digestion of waste activated sludge. J Cleaner Prod 2021; 278.
[22] Qin Y, Yin X, Xu X, Yan X, Bi F, Wu W. Specific surface area and electron donating capacity determine biochar's role in methane production during anaerobic digestion. Bioresour Technol 2020;303:122919.
[23] Lü C, Shen Y, Li C, Zhu N, Yuan H. Redox-active biochar and conductive graphite stimulate methanogenic metabolism in anaerobic digestion of waste-activated sludge: beyond direct interspecies electron transfer. ACS Sustainable Chem Eng 2020;8(33):12626–36.
[24] Kumar M, Dutta S, You S, Luo G, Zhang S, Show PL, et al. A critical review on biochar for enhancing biogas production from anaerobic digestion of food waste and sludge. J Cleaner Prod 2021;305.
[25] Ren S, Usman M, Tsang DCW, Angelidaki OTSI, Zhu X, et al. Hydrochar-facilitated anaerobic digestion: evidence for direct interspecies electron transfer mediated through surface oxygen-containing functional groups. Environ Sci Technol 2020; 54:5755–66.
[26] Wang P, Peng H, Adhikari S, Higgins B, Roy P, Dai W, et al. Enhancement of biogas production from wastewater sludge via anaerobic digestion assisted with biochar amendment. Bioresour Technol 2020;309.
[27] Kaur G, Johnravindar D, Wong JWC. Enhanced volatile fatty acid degradation and methane production efficiency by biochar addition in food waste-sludge co-digestion: A step towards increased organic loading efficiency in co-digestion. Bioresour Technol 2020;308:123250.
[28] Shanmugam SR, Adhikari S, Nam H, Kar Sajib S. Effect of bio-char on methane generation from glucose and aqueous phase of algae liquefaction using mixed anaerobic cultures. Biomass Bioenerg 2018;108:479–86.
[29] Shen R, Jing Y, Feng J, Luo J, Yu J, Zhao L. Performance of enhanced anaerobic digestion with different pyrolysis biochars and microbial communities. Bioresour Technol 2020;296:122354.
[30] Ma H, Hu Y, Kobayashi T, Xu KQ. The role of rice husk biochar addition in anaerobic digestion for sweet sorghum under high loading condition. Biotechnol Rep (Amst) 2020;27:e00515.
[31] Linville JL, Shen Y, Ignacio-de Leon PA, Schoene RP, Urgun-Demirtas M. In-situ biogas upgrading during anaerobic digestion of food waste amended with walnut shell biochar at bench scale. Waste Manag Res 2017;35:669–79.
[32] Qin Y, Wang H, Li X, Cheng JJ, Wu W. Improving methane yield from organic fraction of municipal solid waste (OFMSW) with magnetic rice-straw biochar. Bioresour Technol 2017;245:1058–66.
[33] Deng C, Lin RC, Cheng J, Murphy JD. Can acid pre-treatment enhance biohydrogen and biomethane production from grass silage in single-stage and two-stage fermentation processes? Energy Convers Manage 2019;195:738–47.
[34] Eaton AD, Clesceri LS, Greenberg AE, Franson MAH. Standard methods for the examination of water and wastewater. Am J Public Health Nations Health 1995;56: 387–8.
[35] Wu B, Lin R, Kang X, Deng C, Xia A, Dobson ADW, et al. Graphene addition to digestion of thin stillage can alleviate acidic shock and improve biomethane production. ACS Sustainable Chem Eng 2020;8:13248–60.
[36] B.A. M., H.W. D. Anaerobic fermentations., Bulletin No 321936.
[37] Yin Qianqian, Zhang Bingdong, Wang Ruikun, Zhao Zhenghui. Biochar as an adsorbent for inorganic nitrogen and phosphorus removal from water: a review. Environ Sci Pollut Res Int 2017;24(34):26297–309.
[38] Masebinu SO, Akinlabi ET, Muzenda E, Aboyade AO. A review of biochar properties and their roles in mitigating challenges with anaerobic digestion. Renew Sustain Energy Rev 2019;103:291–307.
[39] Pan J, Ma J, Zhai L, Liu H. Enhanced methane production and syntrophic connection between microorganisms during semi-continuous anaerobic digestion of chicken manure by adding biochar. J Cleaner Prod 2019;240.
[40] Pytlak A, Kasprzycka A, Szafranek-Nakonieczna A, Grzadziel J, Kubaczynski A, Proc K, et al. Biochar addition reinforces microbial interspecies cooperation in methanation of sugar beet waste (pulp). Sci Total Environ 2020;730:138921.
[41] Barua S, Dhar BR. Advances towards understanding and engineering direct interspecies electron transfer in anaerobic digestion. Bioresour Technol 2017;244: 698–707.
[42] Zhao, Z. Li, Y. Quan, X. Zhang. Y.J.W.r. Towards engineering application: Potential mechanism for enhancing anaerobic digestion of complex organic waste with different types of conductive materials. 115; 2017: 266-77.
[43] Rotaru AE, Shrestha PM, Liu F, Markovaite B, Chen S, Nevin KP, et al. Direct interspecies electron transfer between Geobacter metallireducens and Methanosarcina barkeri. Appl Environ Microbiol 2014;80:4599–605.
[44] Jiang Q, Chen Y, Yu S, Zhu R, Zhong C, Zou H, et al. Effects of citrus peel biochar on anaerobic co-digestion of food waste and sewage sludge and its direct interspecies electron transfer pathway study. Chem Eng J 2020;398.
[45] Feng D, Xia A, Liao Q, Nizami AS, Sun C, Huang Y, et al. Carbon cloth facilitates semi-continuous anaerobic digestion of organic wastewater rich in volatile fatty acids from dark fermentation. Environ Pollut 2021;272:116030.
[46] Ma J, Pan J, Qiu L, Wang Q, Zhang Z. Biochar triggering multipath methanogenesis and subdued propionic acid accumulation during semi-continuous anaerobic digestion. Bioresour Technol 2019;293:122026.
[47] Wang G, Li Q, Li Y, Xing Y, Yao G, Liu Y, et al. Redox-active biochar facilitates potential electron tranfer between syntrophic partners to enhance anaerobic digestion under high organic loading rate. Bioresour Technol 2020;298:122524.
[48] Segal JJCL, Martin Jr AE, Conrad CM. An empirical method for estimating the degree of crystallinity of native cellulose using the X-ray diffractometer. Text Res J 1959;29:786–94.
[49] Mohanty Pravakar, Nanda Sonil, Pant Kamal K, Naik Satyanarayan, Kozinski Janusz A, Dalai Ajay K. Evaluation of the physiochemical development of biochars obtained from pyrolysis of wheat straw, timothy grass and pinewood: Effects of heating rate. J Anal Appl Pyrolysis. 2013;104:485–93.
[50] Ma Zhongqing, Yang Youyou, Wu Youlong, Xu Jiajia, Peng Hehuan, Liu Xiaohuan, et al. In-depth comparison of the physicochemical characteristics of bio-char derived from biomass pseudo components: Hemicellulose, cellulose, and lignin. J Anal Appl Pyrol 2019;140:195–204.
[51] Kumar M, Gupta RC, Sharma T. X-ray diffraction studies of Acacia and Eucalyptus wood chars. J Mater Sci 1993;28:805–10.
[52] Sun T, Levin BDA, Schmidt MP, Guzman JJL, Enders A, Martinez CE, et al. Simultaneous Quantification of Electron Transfer by Carbon Matrices and Functional Groups in Pyrogenic Carbon. Environ Sci Technol 2018;52:8538–47.
[53] Özçimen D, Ersoy-Meriçboyu A. Characterization of biochar and bio-oil samples obtained from carbonization of various biomass materials. Renew Energy 2010;35: 1319–24.
[54] Silva CHB, Ferreira DC, Ando RA, Temperini MLA. Aniline-1,4-benzoquinone as a model system for the characterization of products from aniline oligomerization in low acidic media. Chem Phys Lett. 2012;551:130–3.
[55] Sun C, Xia A, Liao Q, Fu Q, Huang Y, Zhu X, et al. Improving production of volatile fatty acids and hydrogen from microalgae and rice residue: Effects of physicochemical characteristics and mix ratios. Appl Energy 2018;230:1082–92.
[56] Blyth RIR, Buqa H, Netzer FP, Ramsey MG, Besenhard JO, Golob P, et al. XPS studies of graphite electrode materials forlithium ion batteries. Appl Surf Sci 2000; 167:99–106.
[57] Miao Z, Huang Y, Xin J, Su X, Sang Y, Liu H, et al. High-Performance Symmetric Supercapacitor Constructed Using Carbon Cloth Boosted by Engineering Oxygen-Containing Functional Groups. ACS Appl Mater Interfaces 2019;11:18044–50.
[58] Qi Y, Ge B, Zhang Y, Jiang B, Wang C, Akram M, et al. Three-dimensional porous graphene-like biochar derived from Enteromorpha as a persulfate activator for sulfamethoxazole degradation: Role of graphitic N and radicals transformation. J Hazard Mater 2020;399:123039.
[59] Schievano A, Berenguer R, Goglio A, Bocchi S, Marzorati S, Rago L, et al. Electroactive Biochar for Large-Scale Environmental Applications of Microbial Electrochemistry. ACS Sustainable Chem Eng 2019;7:18198–212.
[60] Sun T, Levin BD, Guzman JJ, Enders A, Muller DA, Angenent LT, et al. Rapid electron transfer by the carbon matrix in natural pyrogenic carbon. Nat Commun 2017;8:14873.
[61] Lian F, Cui G, Liu Z, Duo L, Zhang G, Xing B. One-step synthesis of a novel N-doped microporous biochar derived from crop straws with high dye adsorption capacity. J Environ Manage 2016;176:61–8.
[62] Liu Y, Dai G, Zhu L, Wang S. Green Conversion of Microalgae into High-Performance Sponge-like Nitrogen-Enriched Carbon. ChemElectroChem 2019;6: 602-.
[63] Li Y, Liu M, Che X, Li C, Liang D, Zhou H, et al. Biochar stimulates growth of novel species capable of direct interspecies electron transfer in anaerobic digestion via ethanol-type fermentation. Environ Res 2020;189.
[64] Cheng Q, Xu C, Huang W, Jiang M, Yan J, Fan G, et al. Improving anaerobic digestion of piggery wastewater by alleviating stress of ammonia using biochar derived from rice straw. Environ Technol Innovation 2020;19.
[65] Zhang P, Zheng S, Liu J, Wang B, Liu F, Feng Y. Surface properties of activated sludge-derived biochar determine the facilitating effects on Geobacter co-cultures. Water Res 2018;142:441–51.
[66] Wang Gaojun, Li Qian, Gao Xin, Wang Xiaochang C. Synergetic promotion of syntrophic methane production from anaerobic digestion of complex organic wastes by biochar: Performance and associated mechanisms. Bioresour Technol 2018;250:812–20.
[67] Pan J, Ma J, Liu X, Zhai L, Ouyang X, Liu H. Effects of different types of biochar on the anaerobic digestion of chicken manure. Bioresour Technol 2018;275:258–65.
[68] Wang D, Ai J, Shen F, Yang G, Zhang Y, Deng S, et al. Improving anaerobic digestion of easy-acidification substrates by promoting buffering capacity using biochar derived from vermicompost. Bioresour Technol 2017;227:286–96.
[69] Cruz Viggi C, Simonetti S, Palma E, Pagliaccia P, Braguglia C, Fazi S, et al. Enhancing methane production from food waste fermentate using biochar: the added value of electrochemical testing in pre-selecting the most effective type of biochar. Biotechnol Biofuels 2017;10:303.
[70] Shen Y, Linville JL, Ignacio-de Leon PAA, Schoene RP, Urgun-Demirtas M. Towards a sustainable paradigm of waste-to-energy process: Enhanced anaerobic digestion of sludge with woody biochar. J Cleaner Prod 2016;135:1054–64.
[71] Fagbohungbe MO, Herbert BM, Hurst L, Li H, Usmani SQ, Semple KT. Impact of biochar on the anaerobic digestion of citrus peel waste. Bioresour Technol 2016; 216:142–9.
[72] Dang Y, Sun D, Woodard T, Wang L-Y, Nevin K, Holmes D. Stimulation of the anaerobic digestion of the dry organic fraction of municipal solid waste (OFMSW) with carbon-based conductive materials. Bioresour Technol 2017;238:30–8.
[73] Wan Z, Sun Y, Tsang DCW, Khan E, Yip ACK, Ng YH, et al. Customised fabrication of nitrogen-doped biochar for environmental and energy applications. Chem Eng J 2020;401.
[74] Zhong K, Li M, Yang Y, Zhang H, Zhang B, Tang J, et al. Nitrogen-doped biochar derived from watermelon rind as oxygen reduction catalyst in air cathode microbial fuel cells. Appl Energy 2019;242:516–25.
[75] Li D, Song L, Fang H, Li P, Teng Y, Li YY, et al. Accelerated bio-methane production rate in thermophilic digestion of cardboard with appropriate biochar: dose-response kinetic assays, hybrid synergistic mechanism, and microbial networks analysis. Bioresour Technol 2019;290:121782.
[76] Zhang M, Li J, Wang Y. Impact of biochar-supported zerovalent iron nanocomposite on the anaerobic digestion of sewage sludge. Environ Sci Pollut Res 2019;26:10292–305.

[77] Dong B, Xia Z, Sun J, Dai X, Chen X, Ni BJ. The inhibitory impacts of nano-graphene oxide on methane production from waste activated sludge in anaerobic digestion. Sci Total Environ 2019;646:1376–84.
[78] Sanna A, Li S, Linforth R, Smart KA, Andresen JM. Bio-oil and bio-char from low temperature pyrolysis of spent grains using activated alumina. Bioresour Technol 2011;102:10695–703.
[79] E.A.S.A. Council. Negative emission technologies: What role in meeting Paris Agreement targets? , EASAC policy report 35, Available on https://easac.eu/publications/details/easac-net/; 2018.
[80] Lin R, O'Shea R, Deng C, Wu B, Murphy JD. A perspective on the efficacy of green gas production via integration of technologies in novel cascading circular bio-systems. Renew Sustain Energy Rev 2021;150.
[81] Davis SJ, Lewis NS, Shaner M, Aggarwal S, Arent D, Azevedo IL, et al. Net-zero emissions energy systems. Science 2018;360.